12-1-2018

In situ atomic layer deposition and electron tunneling characterization of monolayer Al 2 O 3 on Fe for magnetic tunnel junctions

Jamie Wilt

Ryan Goul

Jagaran Acharya

Ridwan Sakidja
Missouri State University

Judy Z. Wu

Recommended Citation

Wilt, Jamie, Ryan Goul, Jagaran Acharya, Ridwan Sakidja, and Judy Z. Wu. "In situ atomic layer deposition and electron tunneling characterization of monolayer Al2O3 on Fe for magnetic tunnel junctions." AIP Advances 8, no. 12 (2018): 125218.

In situ atomic layer deposition and electron tunneling characterization of monolayer Al_2O_3 on Fe for magnetic tunnel junctions

Jamie Wilt,[1] Ryan Goul,[1,a] Jagaran Acharya,[1] Ridwan Sakidja,[2] and Judy Z. Wu[1,a]

[1]*Department of Physics and Astronomy, University of Kansas, Lawrence, Kansas 66045, USA*
[2]*Department of Physics, Astronomy and Materials Science, Missouri State University, Springfield, Missouri 65897, USA*

(Received 4 September 2018; accepted 10 December 2018; published online 20 December 2018)

Magnetic tunnel junctions (MTJs), formed through sandwiching an ultrathin insulating film (so-called tunnel barrier or TB), with ferromagnetic metal electrodes, are fundamental building blocks in magnetoresistive random access memory (MRAM), spintronics, etc. The current MTJ technology employs physical vapor deposition (PVD) to fabricate either amorphous AlOx or epitaxial MgO TBs of thickness around 1 nm or larger to avoid leakage caused by defects in TBs. Motivated by the fundamental limitation in PVD in, and the need for atomically thin and defect-free TBs in MTJs, this work explores atomic layer deposition (ALD) of 1-6 Å thick Al_2O_3 TBs both directly on Fe films and with an ultrathin Al wetting layer. *In situ* characterization of the ALD Al_2O_3 TB was carried out using scanning tunneling spectroscopy (STS). Despite a moderate decrease in TB height E_b with reducing Al wetting layer thicknesses, a remarkable E_b of ~1.25 eV was obtained on 1 Å thick ALD Al_2O_3 TB grown directly on an Fe electrode, which is more than twice of that of thermal AlOx TB (~0.6 eV). Achieving such an atomically thin low-defect TB represents a major step towards improving spin current tunneling in MTJs. https://doi.org/10.1063/1.5054908

I. INTRODUCTION

Magnetic Tunnel Junction (MTJs) are the building blocks for non-volatile magnetoresistive random access memory (MRAM) and are created by sandwiching an ultrathin insulator between two ferromagnetic electrodes.[1–4] MRAM has significant performance and power consumption advantages over standard dynamic random access memory or flash memory with fast read, write times and a memory state which is retained without power draw.[1,2,5] MTJs operate with a differing spin-polarized electron tunneling resistance for parallel and antiparallel magnetization of the ferromagnetic layers. The tunneling current decreases exponentially with the tunnel barrier (TB) thickness and can be further affected due to scattering from defects in TBs. The current MTJ technology based on physical vapor deposition (PVD) employs either amorphous AlOx or epitaxial MgO TBs of thickness around 1 nm or larger to avoid leakage caused by defects in TBs. The TMR values are around 10-70% for AlO_x TBs[6–8] and at least a factor of three higher for crystalline MgO TBs due to enhanced coherent spin current tunneling.[5,9–15] It should be realized that TBs with a smaller thickness approaching atomic scale, that are pinhole-free with low defect concentration are the key to high TMR values desirable for achieving greater signal to noise ratio, lower power consumption, higher speed, and large design margin for device fabrication. Therefore, further reduction of the TB thickness to the sub-nanometer regime remains a major challenge in the research and development of MTJs.

[a]Corresponding Authors: Judy Z. Wu: jwu@ku.edu and Ryan Goul: Ryan.goul1@ku.edu

Atomic layer deposition (ALD) provides a promising alternative to grow low-defect TBs at the atomic-thickness scale for MTJs. ALD is a chemical vapor deposition (CVD) process and has several unique advantages in growth of the TBs for tunnel junctions.[16] First, ALD can provide a highly conformal coating even on high aspect ratio surfaces,[16–18] which is important to minimization of the pinholes and other defects that can cause leakage in TBs. On the other hand, ALD allows atomic-scale accuracy in thickness control due to its self-limiting mechanism. Finally, ALD growth occurs via well-designed chemical ligand exchange between selected pulses of precursors on the sample surface, resulting in minimal un-reacted dangling bonds in the stoichiometric ALD films and hence a very low defect concentration. The low defect-density, high conformality, and excellent thickness control make ALD especially attractive for industrial-scale fabrication of MTJs on large wafers. This has motivated research in ALD growth of TBs for MTJ applications.[19–22] Using *ex situ* ALD deposition, 1.6 nm, or thicker, ALD TBs have been obtained for MTJs, while lower thicknesses produce TBs with pinholes.[20]

The primary challenge in the ALD growth of TBs of sub-nanometer thickness is the formation of an interfacial layer between the metal electrode and the dielectric ALD TB, typically formed when the metal surface is exposed to ambient or low vacuum in *ex situ* processes. This defective interface has a profound effect on the ALD dielectric film quality. For example, the dielectric constant (ε_r) is significantly reduced from the bulk single crystals values when the ALD film thickness is on the order of tens of nanometers or lower,[23–27] indicative a high defect concentration in ALD dielectric films grown on defective metal-insulator interfaces. Even in the *in situ* ALD process, a prolonged exposure to vacuum (even at high vacuum of $\sim 10^{-7}$ Torr) during heating of a metal electrode for ALD TB growth can cause formation of such an interface.[27] This interface is even more detrimental to ALD TBs for MTJs since the additional TB defects can impair spin current tunneling current in MTJs.[24,26,27] In a recent work, we reported a dynamic heating process for *in situ* ALD TB growth which is capable of growing high quality ALD Al_2O_3 TBs on aluminum at the monolayer scale with an excellent control of the Al-Al_2O_3 interface to a negligible level.[23,28–31] A key step is in control of the hydroxylation of the metal surface during the first monolayer growth of ALD Al_2O_3.[23,31] This control leads to an order of magnitude reduction in ALD Al_2O_3 TB thickness, from 1 nm to about 1 Å, and the dielectric constant of ALD Al_2O_3 films of 3 nm in thickness comparable to that of the bulk Al_2O_3 single crystals.

While atomically thin ALD Al_2O_3 TBs may be promising for MTJs, two fundamental issues are present in growth of the ALD Al_2O_3 TBs on ferromagnetic electrodes. An Al wetting layer on the ferromagnetic metal electrode, such as Fe, is expected to reduce the TMR value by incoherently scattering the spin-polarized electron tunneling.[32] This means that the Al wetting layer should be as thin as possible since it is not a ferromagnetic material. This, however, may affect hydroxylation of the electrode surface and lead to defective nucleation of the ALD Al_2O_3 on the Al/Fe or Fe film directly. An in-depth understanding of the nucleation and evolution of the ALD Al_2O_3 TBs of sub-nanometer in thickness on Fe films with Al wetting layers of different thicknesses is therefore important to development of MTJs with ALD TBs. In this work, in situ Scanning Tunneling Spectroscopy (STS) was employed to characterize the electron tunneling properties of ALD Al2O3 TBs with thicknesses ranging from 1-6 Å in order to inspect TB quality, via barrier height measurement, as the Al layer was systematically reduced from 7 nm to zero. In tandem, *Ab initio* Molecular Dynamics (AIMD) simulations were carried out to examine the possibility of adapting the pre-ALD H_2O pulse to produce a uniform layer of OH groups directly on the Fe surface.

II. METHODS

To create the metal-insulator structure for *in situ* STS, a trilayer of Nb (50 nm)/Fe (20 nm)/Al (0-7 nm) was DC magnetron sputtered using Argon in vacuum chambers with base pressures between 1.5 - 5.5 × 10^{-7} Torr onto an Au (50 nm) coated SiO_2/Si substrate at deposition rates of 1.7 nm/s (330 W 14 mTorr), 1.0 nm/s (200W 4 mTorr), and 0.5 nm/s (90 W 14 mTorr) respectively, which were all previously empirically estimated. A washer was clamped to the Au surface of the substrate to create a connection between the sample and the STS ground. The niobium layer served to prevent diffusion between the Al and Au layers which may cause significant problems with ALD nucleation

in thinner Al films. In order to understand the role of the Al wetting layer thickness, five different Al thicknesses of 7 nm, 4 nm, 2 nm, 1 nm and 0 nm were selected in this work. After metal sputtering, the samples were transferred *in situ* to the ALD chamber under high vacuum where a pre-ALD H_2O pulse of 2s in duration to hydroxylate the metal surface, which was followed with a N_2 purge for 35s and a trimethylaluminum (TMA) pulse of 1s to form a monolayer of Al_2O_3 using the optimized ALD conditions discussed in our previous papers.[30,31] With an additional N_2 purge, one cycle of ALD growth of an Al_2O_3 monolayer was completed with the layer thickness of about 1.1-1.2 Å.[16,25,29,33] In this study, up to five cycles of ALD Al_2O_3 TBs were grown on metal electrodes. After ALD, the samples were *in situ* transferred under high vacuum to the STS chamber which had a pressure of about $1x10^{-9}$ Torr. *dI/dV* spectra were taken over 100-200 random locations on the sample's surface using a mechanically-cleaved Pt-Ir tip with a voltage modulation of 30 mV at 5 kHz and a set point of 2 V, 200 pA. This same tip was used to acquire all *dI/dV* spectra in this experiment except for a one of the final sets of data where the new tip was checked to assure it was comparable in quality to the previous tip.[34] The TB height was estimated by the intersection of two bisquare-method linear fits to ln(*dI/dV*) and the ALD coverage was defined as the percentage of locations which had *dI/dV* with calculated E_b values greater than 0.8 eV.[30,31] *Ab-initio* molecular dynamics (AIMD) simulations for H_2O molecules on the Fe (100), Fe (110), and Fe (111) surface were conducted under a constant volume and temperature ensemble as implemented in VASP code.[35] The Fe slabs were constructed using experimentally determined lattice parameters[36] and were adjusted in size to accommodate thermal expansion. A "water pool" was added to the top site of each Fe surface to simulate the pre-ALD H_2O pulse. Additional details for the simulation procedure can be found in our previous works.[30,31]

III. RESULTS AND DISCUSSION

Figure 1a illustrates schematically the samples fabricated using the procedures described earlier. Figure 1b shows the sequential ligand exchanges between pulses of H_2O and TMA in one ALD cycle which leads to one atomic layer of Al_2O_3 of thickness ~1.1-1.2 Å.[37,38] To achieve 6 Å ALD Al_2O_3 TB thickness, five ALD growth cycles were carried out. This fabrication was all done *in situ* using a specialized STS sample stage with the bias voltage applied between the STS tip and the Au bottom contact electrode, which is shown in Figure 1c.

Figures 2a and 2b show representative dI/dV spectra taken on the Nb (50 nm)/Fe (20 nm)/Al (7 nm)/ALD Al_2O_3 (1 Å) and Nb (50 nm)/Fe (20 nm)/ALD Al_2O_3 (1 Å) respectively. Qualitatively, a similar nonlinear trend can be observed on both spectra, illustrating tunneling through the ALD Al_2O_3 TB of 1 Å thickness with or without the Al wetting layer. The fitting (red lines) to the band gap region and the conduction band region allows extraction of TB height E_b at the intersection of the fitting lines. The E_b for the sample with a 7 nm Al wetting layer (Figure 2a) is ~1.66 eV, which is consistent with the range we measured on Nb (20 nm)/Al (7 nm)/ALD Al_2O_3 (1 Å) samples earlier without an Fe layer in the electrode stack.[30,31] This indicates a thick 7 nm Al wetting layer would thoroughly cover the surface of the underlying metal, either Nb or Fe. A lower E_b ~1.25 eV was observed on Nb (50 nm)/Fe (20 nm)/ALD Al_2O_3 (1 Å) (Figure 2b), which reveals that the difference on the surface of Al and Fe sensitively affects the ALD Al_2O_3 nucleation and will be discussed in detail later. When the Al wetting layer was varied within the range of 0-7 nm, the E_b of the ALD Al_2O_3 TB (1 Å) was found to remain constant in the Al thickness range of 4-7 nm, followed by a decrease when the Al thickness was further reduced below 4 nm, together with a drop in the ALD coverage from 96% to 93.9% (Figure 2c). The reduced E_b values indicate an increased defect concentration in the ALD Al_2O_3 TB (1 Å), possibly due to the difference in the nucleation of the ALD Al_2O_3 on Fe as compared to Al assuming the surface of the Fe may not be fully covered at smaller Al wetting layer thicknesses due possibly to intermetallic diffusion or surface roughness (1.2 - 1.4 nm) causing gaps in Al coverage. However, these effects are not significant. With 1 nm thick Al wetting layer, the E_b ~1.44 eV is still in the range of high quality ALD Al_2O_3 TB (1 Å) and significantly better than the E_b ~1.0 eV observed on ALD Al_2O_3 TB (1 Å) with a defective Al-Al_2O_3 interfacial layer.[30] Comparatively, the E_b values are in the range of 0.5-0.7 eV and 0.4-0.9 eV for thermal AlOx TBs and epitaxial MgO TBs respectively,[5,39,40] due to the presence of defects such as oxygen vacancies.

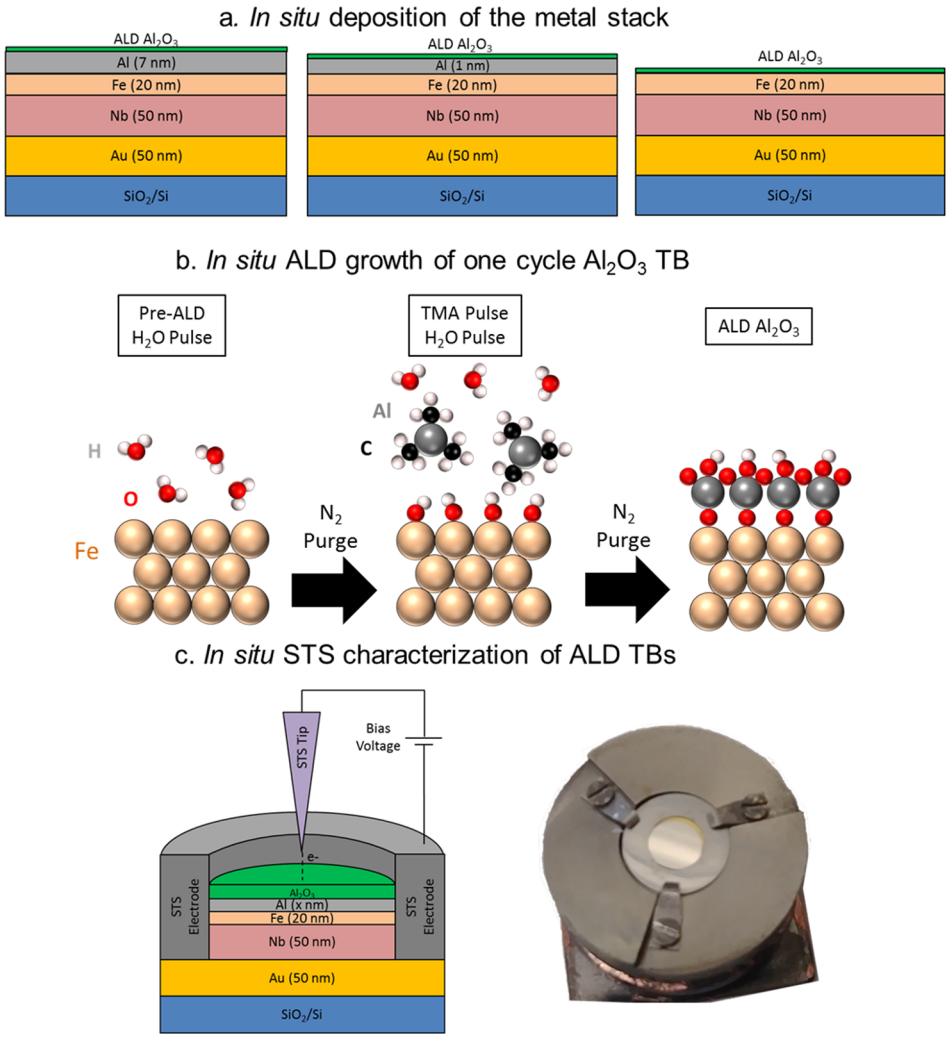

FIG. 1. (a) diagrammatic representation of samples fabricated with varying Al wetting layer thickness, followed by ALD deposition of Al_2O_3. (b) Representation of ALD process involving alternating precursors (H_2O and TMA) with vacuum purges in-between precursor exposures. (c) A cross-sectional representation of how samples in this experiment are grown and analyzed via *in situ* STS. Pictured next to this diagram is an actual picture of a sample in the sample stage where the clamped down washer is the STS electrode.

Therefore, the observation of higher E_b values in 1 Å thick ALD Al_2O_3 TB, as opposed to their PVD counterparts with at least 5-10 times larger thickness, illustrates the promising potential of the ALD approach for synthesis of high-quality, sub-nm thick TBs for MTJ applications.

Figure 2d depicts the E_b and coverage of ALD Al_2O_3 TBs as function of the ALD cycle number in the range of 1-5 (or TB thickness in the range of 1-6 Å) on the Nb (50 nm)/Fe (20 nm)/Al (1 nm)/ALD Al_2O_3 samples. A constant E_b and ALD coverage were observed in the Al_2O_3 TB thickness range of 1-6 Å, which indicates that the ALD Al_2O_3 TB is fairly uniform. This means that the reduced E_b value of the ALD Al_2O_3 TBs on Fe or on Fe with a very thin Al wetting layer is unlikely to be caused by the formation of an FeO_x interface since a defective FeO_x IL would reduce E_b more significantly at a smaller TB thickness, resulting in a thickness-dependent E_b.[30] This observation is important since a defective interfacial layer is highly detrimental to the TB quality, but can be minimized in the *in situ* ALD process with well controlled growth conditions. Therefore, the observation of the reduced E_b value of the ALD Al_2O_3 TBs grown on Fe without or with a very thin Al wetting layer raises a question on the difference in nucleation of the ALD Al_2O_3 on Fe with respect to Al.

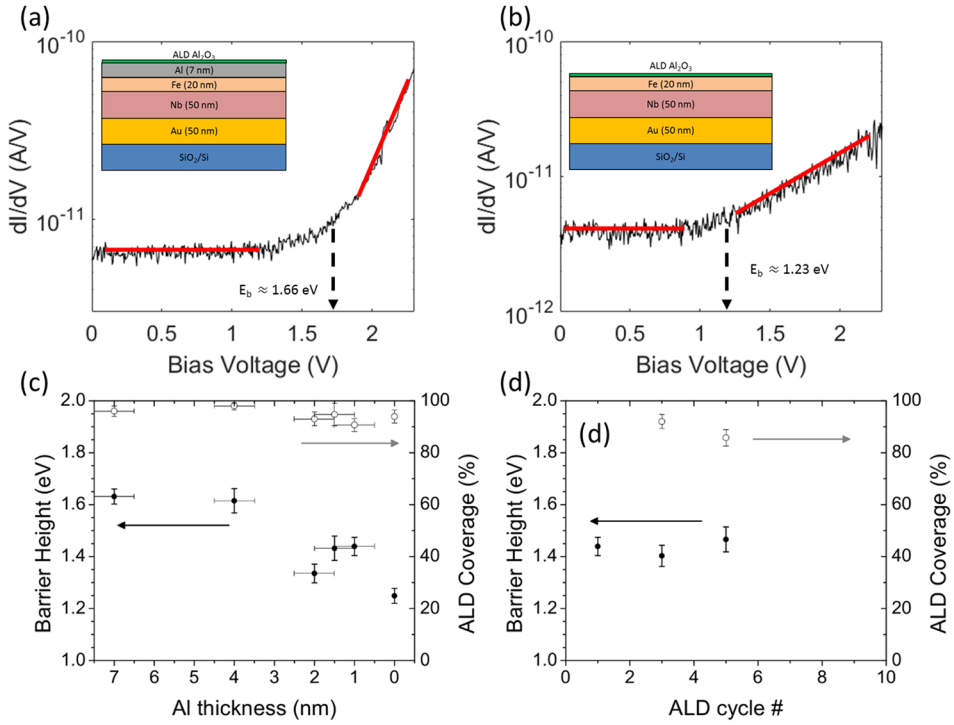

FIG. 2. Al_2O_3 was deposited using *in situ* ALD on a Fe/Al surface. Representative *dI/dV* spectra are shown (in log scale) with linear fit lines traced over the band gap and conduction band regions of the spectra; their intersection point is used to estimate E_b for (a) 1c ALD Al_2O_3 grown on a 7 nm Al wetting layer, and for (b) 1c ALD Al_2O_3 grown directly on Fe. (c) E_b and ALD coverage were estimated for samples with 1 cycle of ALD Al_2O_3 deposited on Al with varying thickness and for samples with (d) ALD Al_2O_3 of varying thickness deposited on a 1 nm Al layer. The inserts depict the layered structure which was deposited.

To shed light on the differences of Fe and Al surfaces for ALD oxide growth, AIMD simulations were carried out to examine the growth kinetics of ALD Al_2O_3 on Fe in comparison with on Al as we reported previously.[30,31] Considering hydroxylation of the metal surface during the first H_2O pulse is the most critical step in nucleation of the monolayer ALD Al_2O_3, Figure 3 illustrates this process on Fe surfaces of (110), (100) and (111) orientations, respectively. The first two are energetically preferred in polycrystalline Fe films and have smaller inter-Fe atom distance on the surface than in the (111) Fe case. The AIMD simulation suggests that a hydroxylated Fe surface is possible within the first H_2O pulse. However, the effectiveness in generating adsorbed hydroxyl groups (OH_{ads}) without dissociation of H_2O into oxygen and hydrogen is dependent on the Fe surface orientation. The Fe (110) and Fe (100) surfaces both result in OH_{ads} creation without much oxygen formation whereas the Fe (111) surface leads to a high amount of oxygen. As we have shown earlier on the Al surface, a primary mechanism dictating the H_2O dissociation into OH_{ads} is the inter-molecular interaction between H_2O molecules attached to the metal surface during the first H_2O pulse. At an optimal pre-ALD H_2O pulse duration to enable an adequate concentration of H_2O molecules on a metal surface, the inter-atomic distance of metal atoms on the surface plays an important role in affecting the inter-molecular interaction between H_2O molecules attached to the metal atoms and their dissociation paths.

The FCC structured Al (111) facet is one of the favorable surfaces with a high density of surface atoms (0.143 atoms/Å^2), which leads to strong inter-molecular interaction between H_2O molecules and facilitates their dissociation into OH_{ads} on the Al surface. In contrast, Fe has a BCC structure.[41,42] Although the surface densities of 0.122 and 0.155 atoms/Å^2 on (100) and (110) facets respectively are excellent for the dissociation of H_2O molecules into OH_{ads}, the much reduced surface density of 0.063 atoms/Å^2 on (111) Fe may lead to reduced efficiency for such a dissociation. Consequently, the ALD Al_2O_3 on Fe or on Fe with very thin Al may have lower density on average. In addition,

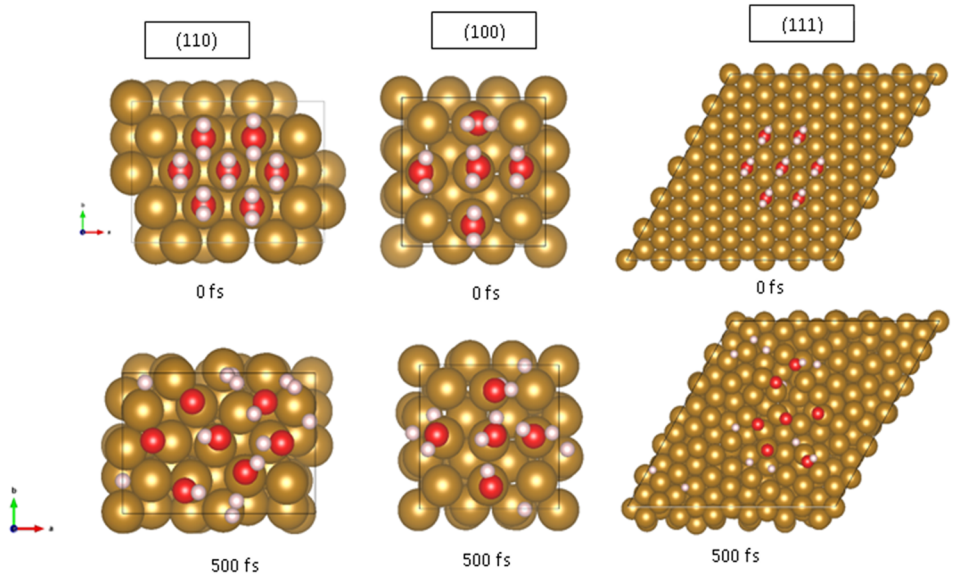

FIG. 3. Snapshots from AIMD simulations are shown for a water pool placed on a Fe (110), Fe (100) and Fe (111) surface at 473 K for times up to 500 fs.

the FeO_x IL from the pre-ALD H_2O pulse may form on the Fe (111) if H_2O molecules cannot efficiently dissociate to OH_{ads}, and rather to hydrogen and oxygen that may react with Fe to form an FeO_x IL. This explains the reduced ALD Al_2O_3 TB coverage on Fe surface without an Al wetting layer or with a very thin Al wetting layer.

Figure 4a shows that the non-ALD dI/dV spectra. Overall, these spectra share similar characteristics of flatness and a rounded conduction band onset for samples with 7, 1, and 0 nm (on Fe) thick Al wetting layers while the E_b values are significantly lower than that of the ALD TBs. This indicates that though the substrate makeups are different, many of these lower quality spots in the film are similar in composition. The low E_b values in the range of 0.4-0.6 eV, which are comparable to the E_b values measured on thermal AlOx TBs,[30] suggested that the non-ALD TBs formed on these spots are most probably defective AlOx TBs on FeOx IL/Fe (111) based on the simulation result in Figure 3. Nevertheless, after viewing the distributions in Figure 4b, and the coverage rates from Figure 2c, the percentage of the surface that is defective/lower quality increases with decreasing Al

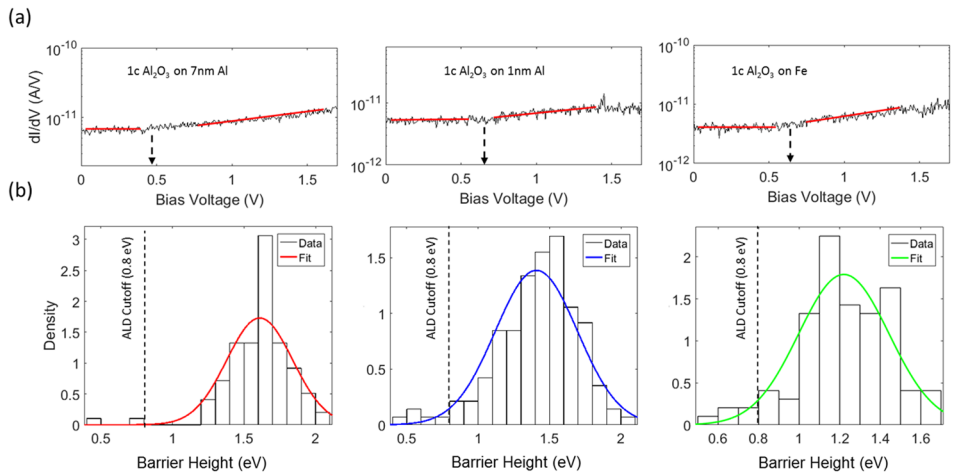

FIG. 4. (a) examples of lower-quality non-ALD dI/dV spectra on 7nm Al, 1 nm Al, and directly on Fe. (b) Distributions of barrier heights with a normal distribution fit to them, a dashed line has been drawn at the barrier height cut-off value 0.8 eV.

wetting layer thickness. Additionally, some of these defective surface spectra have increased noise and do not appear similar to those from Figure 4a possibly indicating different types of defects in the samples with very thin or no wetting layer. Intuitively, one would think that any exposure to heat and H_2O molecules would cause oxidation in an Fe film based on how we expect Fe films to behave *ex situ*. Indeed, even *in situ*, the heating of the Fe film, its exposure to H_2O during the first ALD pulse, and trace O_2 all have the potential to create FeOx.[43] However, our result indicates this does not appear to have happened to any significant level with a well-controlled *in situ* ALD process, especially the initial hydroxylation of the Fe surface, to minimize FeOx IL formation. In addition, a further improved ALD TB may be achieved on epitaxial Fe films with desired facets of (100) and (110).

To quantify to what degree the FeOx IL formation occurs when *in situ* ALD Al_2O_3 is grown on Fe, ALD Al_2O_3 TBs were grown on Fe with varying cycle numbers. STS reveals, in Figure 5a, a nearly constant coverage of the ALD TB on the Fe surface with a 5% increase of E_b from 1.25 eV to 1.31 eV with the increasing ALD cycle number from 1 to 5. Our previous work[30] and the data from Figure 2b show a constant barrier height with increasing cycle number can be obtained on Al surface with a negligible IL. Considering the 5% increases in the E_b value in the ALD cycle number range of 1-5 is small, we argue the FeOx IL is unlikely significant in the ALD Al_2O_3 TBs grown directly on Fe. This observation is therefore important to the potential implementation of ALD TBs with sub-nm thickness into tunnel junction devices. Furthermore, despite the almost constant E_b values at different TB thicknesses, an E_b value of 1.25-1.31 eV for ALD Al_2O_3 TBs on Fe is lower than the same TB on Al[30,31] by about 25-30%. Considering the IL effect is unlikely significant, we hypothesize the lower E_b value of the ALD Al_2O_3 TBs on Fe may relate to the lower density of the ALD Al_2O_3 nucleate on BCC Fe (100) and (111) surfaces with smaller densities of surface atoms, as compared to that on the FCC Al (111) surface. Confirmation of this hypothesis is certainly important to development of atomically thin and low-defect ALD dielectric on metal and semiconductor surfaces.

To rule out the possibility that this lower E_b value of the ALD Al_2O_3 TBs on Fe was due to un-optimized ALD growth condition originally optimized for ALD Al_2O_3 TBs on the Al surface, three different dynamic heating times of 13, 15, and 17 minutes were tested, which primarily reduced the pre-ALD heating time of the Fe film and also the initial ALD temperatures to 175, 190, and 200 °C, respectively, at the same fixed heating power.[31] From Figure 5b, the 15 minutes heating gave the optimal result with an E_b of 1.25 ± 0.03 eV and ALD coverage of 93.9 ± 2.4%. At 13 minutes of heating with 175 °C as the starting temperature, less OH groups are expected to form on the Fe surface, frustrating the ALD process. When the heating time was 17 minutes with an initial temperature of 200 °C, it is possible that there is more FeOx formation due to the dissociation of OH and H_2O molecules into O atoms.[30,31] This result shows that the ALD conditions ALD Al_2O_3 TBs are nearly identical although the Fe and Al may have different properties, such as adsorption energies and surface atom density. In other words, the cause of the reduced E_b value on an Fe surface is most

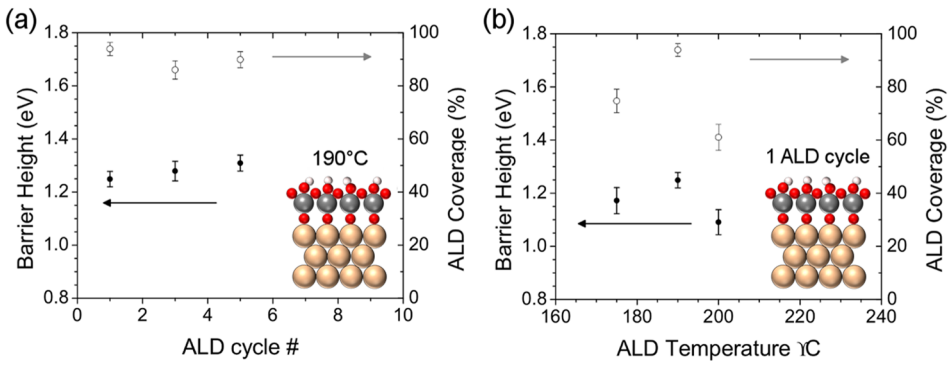

FIG. 5. An STS study on the growth of ALD Al_2O_3 on Fe. (a) A varying number of ALD cycles were deposited directly on the Fe in the configuration shown in the insert. (b) One cycle of ALD Al2O3 was grown on Fe at varying ALD temperatures. The tunnel barrier height E_b is shown in the solid points and the ALD coverage in the hollow points.

probably the lower density of the ALD Al_2O_3 TBs nucleated on BCC Fe surface due to the lower density of the surface atoms as compared to its counterpart on FCC Al surface.

IV. CONCLUSIONS

In conclusion, we report the first success in growth of atomically thin (1-6 Å in thickness), low-defect ALD Al_2O_3 TBs through atomic layer deposition directly on ferromagnetic Fe electrode. *In situ* STS studies have confirmed that high E_b up to 1.25 eV can be obtained on the 1 Å thick ALD Al_2O_3 TBs grown directly on Fe, which is more than twice of that of the thermal AlOx TBs. This indicates a significantly lower defect concentration can be obtained in the former, in addition to an order of magnitude reduction in the TB thickness. While Al wetting layer may provide a slightly better nucleation surface for the ALD Al_2O_3 TBs as reflected in up to ~30% improvement in the E_b, we have found that this wetting layer is not necessary for high quality ALD Al_2O_3 TBs to deposited directly on Fe electrode with a coverage of 94%, a slight decrease from 96% with an Al wetting layer. AIMD simulations of H_2O molecules on the Fe (100), Fe (110), and Fe (111) surfaces during the pre-ALD H_2O pulse reveal that the hydroxylation of the first two Fe surfaces, which are energetically more preferred orientations in polycrystalline Fe films, can be facilitated by a stronger inter-H_2O molecule interaction as H_2O molecules attached to the Fe atoms of shorter inter-atom distances. This is in contrast to the weakened inter-H_2O molecule interaction on Fe (111) surface at a larger inter-atom distance, which may lead to detrimental dissociation of the H_2O molecules into oxygen and hydrogen and hence formation of FeO_x interfacial layer. Considering a possible small volume portion of Fe (111) may exist in the polycrystalline Fe films used in this study, a higher coverage of the ALD Al_2O_3 TBs on epitaxial (100) and (110) Fe films is expected. Therefore, this work demonstrates that the fundamental roadblock towards achieving MTJs with atomically thin, defect-free dielectric TBs can be removed using the ALD TB approach.

ACKNOWLEDGMENTS

The authors acknowledge support in part by US Army Research Office Contract ARO-W911NF-16-1-0029 and National Science Foundation Contracts NSF-DMR-1337737 and NSF-DMR-1508494.

[1] C. Chappert, A. Fert, and F. N. Van Dau, Nature Materials **6**(11), 813 (2007).
[2] A. Hirohata and K. Takanashi, J. Phys. D: Appl. Phys. **47**(19), 193001 (2014).
[3] J.-G. Jimmy Zhu and C. Park, Mater. Today **9**(11), 36 (2006).
[4] I. Žutić, J. Fabian, and S. Das Sarma, Reviews of Modern Physics **76**(2), 323 (2004).
[5] S. Yuasa, T. Nagahama, A. Fukushima, Y. Suzuki, and K. Ando, Nature Materials **3**(12), 868 (2004).
[6] T. Miyazaki and N. Tezuka, J. Magn. Magn. Mater. **139**(3), L231 (1995).
[7] J. S. Moodera, L. R. Kinder, T. M. Wong, and R. Meservey, Phys. Rev. Lett. **74**(16), 3273 (1995).
[8] D. Wang, C. Nordman, J. M. Daughton, Z. Qian, and J. Fink, IEEE Transactions on Magnetics **40**(4), 2269 (2004).
[9] S. S. P. Parkin, C. Kaiser, A. Panchula, P. M. Rice, B. Hughes, M. Samant, and S.-H. Yang, Nature Materials **3**(12), 862 (2004).
[10] S. Yuasa, Y. Suzuki, T. Katayama, and K. Ando, Appl. Phys. Lett. **87**(24), 242503 (2005).
[11] Z. Bai, L. Shen, Q. Wu, M. Zeng, J.-S. Wang, G. Han, and Y. P. Feng, Physical Review B **87**(1), 014114 (2013).
[12] Y. Jang, C. Nam, K.-S. Lee, B. K. Cho, Y. J. Cho, K.-S. Kim, and K. W. Kim, Appl. Phys. Lett. **91**(10), 102104 (2007).
[13] Y. Ke, K. Xia, and H. Guo, Phys. Rev. Lett. **105**(23), 236801 (2010).
[14] K. Komagaki, M. Hattori, K. Noma, H. Kanai, K. Kobayashi, Y. Uehara, M. Tsunoda, and M. Takahashi, IEEE Transactions on Magnetics **45**(10), 3453 (2009).
[15] A. K. Rumaiz, J. C. Woicik, W. G. Wang, J. Jordan-Sweet, G. H. Jaffari, C. Ni, J. Q. Xiao, and C. L. Chien, Appl. Phys. Lett. **96**(11), 112502 (2010).
[16] S. M. George, Chem. Rev. **110**(1), 111 (2009).
[17] S. D. Elliott, Semicond. Sci. Technol. **27**(7), 074008 (2012).
[18] G. A. Malek, E. Brown, S. A. Klankowski, J. Liu, A. J. Elliot, R. Lu, J. Li, and J. Wu, ACS Applied Materials & Interfaces **6**(9), 6865 (2014).
[19] S. Fabretti, R. Zierold, K. Nielsch, C. Voigt, C. Ronning, P. Peretzki, M. Seibt, and A. Thomas, Appl. Phys. Lett. **105**(13), 132405 (2014).
[20] X. Liu and J. Shi, Appl. Phys. Lett. **102**(20), 202401 (2013).
[21] R. Mantovan, S. Vangelista, B. Kutrzeba-Kotowska, S. Cocco, A. Lamperti, G. Tallarida, D. Mameli, and M. Fanciulli, Thin Solid Films **520**(14), 4820 (2012).
[22] R. Mantovan, S. Vangelista, B. Kutrzeba-Kotowska, A. Lamperti, N. Manca, L. Pellegrino, and M. Fanciulli, J. Phys. D: Appl. Phys. **47**(10), 102002 (2014).

[23] J. Acharya, J. Wilt, B. Liu, and J. Wu, ACS Applied Materials & Interfaces **10**(3), 3112 (2018).
[24] H. Birey, J. Appl. Phys. **48**(12), 5209 (1977).
[25] M. D. Groner, J. W. Elam, F. H. Fabreguette, and S. M. George, Thin Solid Films **413**(1), 186 (2002).
[26] H. Kim and P. C. McIntyre, Journal of the Korean Physical Society **48**(1), 5 (2006).
[27] K. Y. Lee, Y. J. Lee, P. Chang, M. L. Huang, Y. C. Chang, M. Hong, and J. Kwo, Appl. Phys. Lett. **92**(25), 252908 (2008).
[28] A. J. Elliot, G. Malek, L. Wille, R. Lu, S. Han, J. Z. Wu, J. Talvacchio, and R. M. Lewis, IEEE Transactions on Applied Superconductivity **23**(3), 1101405 (2013).
[29] A. J. Elliot, G. A. Malek, R. Lu, S. Han, H. Yu, S. Zhao, and J. Z. Wu, Rev. Sci. Instrum. **85**(7), 073904 (2014).
[30] J. Wilt, Y. Gong, M. Gong, F. Su, H. Xu, R. Sakidja, A. Elliot, R. Lu, S. Zhao, and S. Han, Physical Review Applied **7**(6), 064022 (2017).
[31] J. Wilt, R. Sakidja, R. Goul, and J. Z. Wu, ACS Applied Materials & Interfaces **9**(42), 37468 (2017).
[32] S. Yuasa and D. D. Djayaprawira, J. Phys. D: Appl. Phys. **40**(21), R337 (2007).
[33] C. Barbos, D. Blanc-Pelissier, A. Fave, C. Botella, P. Regreny, G. Grenet, E. Blanquet, A. Crisci, and M. Lemiti, Thin Solid Films **617**, 108 (2016).
[34] C. Julian Chen, *Introduction to Scanning Tunneling Microscopy* (Oxford University Press, 1993).
[35] J. Hafner, J. Comput. Chem. **29**(13), 2044 (2008).
[36] H.-K. Mao, W. A. Bassett, and T. Takahashi, J. Appl. Phys. **38**(1), 272 (1967).
[37] R. Lu, A. J. Elliot, L. Wille, B. Mao, S. Han, J. Z. Wu, J. Talvacchio, H. M. Schulze, R. M. Lewis, D. J. Ewing, H. F. Yu, G. M. Xue, and S. P. Zhao, IEEE Transactions on Applied Superconductivity **23**(3), 1100705 (2013).
[38] A. W. Ott, J. W. Klaus, J. M. Johnson, and S. M. George, Thin Solid Films **292**(1), 135 (1997).
[39] T. Kiyomura, Y. Maruo, and M. Gomi, J. Appl. Phys. **88**(8), 4768 (2000).
[40] S. Mitani, T. Moriyama, and K. Takanashi, J. Appl. Phys. **93**(10), 8041 (2003).
[41] F. M. Mulder, B. Assfour, J. Huot, T. J. Dingemands, M. Wagemaker, and A. J. Ramirez-Cuesta, The Journal of Physical Chemistry **114**(23), 10648 (2010).
[42] I. G. Wood, L. Vodadlo, D. P. Dobson, G. D. Price, A. D. Fortes, F. J. Cooper, J. W. Neale, A. M. Walker, W. G. Marshall, M. G. Tucker, D. J. Francis, H. J. Stone, and C. A. McCammon, J. Appl. Crystallogr. **41**(5), 886 (2008).
[43] R. M. Cornell and U. Schwertmann, *The Iron Oxides Structure, Properties, Reactions, Occurrences and Uses* (Wiley-VCH, 2003).